USCAP

Check for updates

ARTICLE

PLOD3 regulates the expression of YAP1 to affect the progression of non-small cell lung cancer via the PKCδ/CDK1/LIMD1 signaling pathway

Wei-Hao Li[1,2], Kai Huang[1,2], Feng-Biao Wen[1], Guang-Hui Cui[1], Hai-Zhou Guo[1] and Song Zhao[1✉]

Procollagen-lysine, 2-oxoglutarate 5-dioxygenase (PLOD3) is a crucial oncogene in human lung cancer, whereas protein kinase C δ (PKCδ) acts as a tumor suppressor. In this study, we aimed to explore the regulation by PLOD3 on the expression of YAP1 to affect the progression of non-small cell lung cancer (NSCLC) via the PKCδ/CDK1/LIMD1 signaling pathway. We found that PLOD3, CDK1, and YAP1 were highly expressed, while LIMD1 was poorly expressed in NSCLC tissues. Mechanistic investigation demonstrated that silencing PLOD3 promoted the cleavage of PKCδ in a caspase-dependent manner to generate a catalytically active fragment cleaved PKCδ, enhanced phosphorylation levels of CDK1, and LIMD1 but suppressed nuclear translocation of YAP1. Furthermore, functional experimental results suggested that loss of PLOD3 led to increased phosphorylation levels of CDK1 and LIMD1 and downregulated YAP1, thereby suppressing the proliferation, colony formation, cell cycle entry, and resistance to apoptosis of NSCLC cells in vitro and inhibiting tumor growth in vivo. Taken together, these results show that PLOD3 silencing activates the PKCδ/CDK1/LIMD1 signaling pathway to prevent the progression of NSCLC, thus providing novel insight into molecular targets for treating NSCLC.

INTRODUCTION

Lung cancer was estimated to be responsible for 25% of cancer-related deaths in 2019, accompanied by a dismal five-year survival rate of only 19%[1]. Non-small cell lung cancer (NSCLC) is the most prevalent type of lung cancer, accounting for approximately 80-90% of all lung cancers[2]. The first-line treatment options of NSCLC are comprised of chemotherapy, targeted therapies, and pem-brolizumab treatment in patients with high PD-L1 expression[3]. However, the overall cure and survival rates for NSCLC remain low. Therefore, investigation to further understand the disease pathology and mechanisms of NSCLC progression are required for the development of new, more effective therapies[4].

Procollagen-lysine, 2-oxoglutarate 5-dioxygenase (PLOD3) is a membrane-bound homodimeric enzyme that hydroxylates lysyl residues in collagen-like peptides, thus acting as an effective initiator of lung cancer metastasis, while also presenting a promising therapeutic target to improve the survival of lung cancer patients[5]. PLOD3 overexpression is common in gastric, colorectal, and pancreatic cancers, and it promotes tumor progression and poor prognosis in gliomas. PLOD3 promotes lung metastasis *via* regulation of the transcription factor signal transducer and activator of transcription 3 (STAT3). Many studies have suggested the involvement of protein kinase c-delta (PKCδ) in the activations of p38 and mitogen-activated protein kinase (MAPK) in heart failure[5,6]. A recent study has reported that inhibition of PLOD3 displays anti-tumor activity in human lung

cancer cells by regulating the PKCδ signaling pathway[7]. PKCδ has been revealed to play bi-functional role in regulating cell death and proliferation[8], which has been reported to aggravate the progression of NSCLC[9]. Results of a previous study showed that PKCδ can be cleaved to a constitutively active catalytic fragment (PKCδ-cat) in a caspase-dependent manner, which promotes the phosphorylation of cyclin-dependent kinase 1 (CDK1)[10]. In turn, CDK1 has been reported to participate in the regulatory axis involving the suppression by the anteoneoplastic alkaloid lycorine of NSCLC cell growth[11]. Further, CDK1 has been documented to induce phosphorylated (p)-LIM domain-containing protein 1 (LIMD1)[12]. LIMD1 functions as an important tumor suppressor in the development of human lung cancer[13], and is furthermore a survival prognostic marker of gastric cancer that hinders tumor progression by suppressing the activation of YAP1. Overexpression of LIMD1 impeded the tumor growth, cell motility, invasiveness, and metastasis of gastric cancer, whereas knockdown of LIMD1 promoted these cellular phenotypes[14]. Besides, LIMD1 can inhibit the activation of its downstream factor, Yes-associated protein 1 (YAP1), as well as the intracellular translocation of YAP1[14]. YAP1, as a prognostic predictor in various tumors, has been reported to be correlated with poor prognosis of NSCLC[15]. Additionally, YAP1 is an oncogenic member of the Hippo signaling pathway, which promotes self-renewal and angiogenesis of NSCLC cells[16]. CDK1 phosphorylation of YAP promotes mitotic defects and increases cell motility, and is essential for neoplastic transformation[17].

[1]Department of Thoracic Surgery, The First Affiliated Hospital of Zhengzhou University, Zhengzhou 450052, P.R. China. [2]These authors contributed equally: Wei-Hao Li, Kai Huang. ✉email: diqbhunuhdwui@163.com

From the findings above, we hypothesized that PLOD3 should exert crucial effects on the progression of NSCLC through regulation of the PKCδ/CDK1/LIMD1/YAP1 axis. We understood a series of experiments in vitro and in vivo to test this hypothesis, and to provide novel insight into the specific mechanisms underlying the progression of NSCLC.

MATERIALS AND METHODS
Bioinformatics analysis
NSCLC-related dataset GSE19188, retrieved from the GEO database (https://www.ncbi.nlm.nih.gov/geo/), contains 65 normal samples and 91 cancer samples. The probe ID of the dataset was converted into Gene Symbol through the platform annotation file GPL570 [HG-U133_Plus_2] Affymetrix Human Genome U133 Plus 2.0 Array. Gene differential expression was analyzed by the R language "limma" package (http://www.bioconductor.org/packages/release/bioc/html/limma.html), with $p < 0.001$ sets as the screening criterion. The R language "pheatmap" package (https://cran.r-project.org/web/packages/pheatmap/index.html) was used to draw differential gene expression heat maps. NSCLC-related genes were predicted using the CTD (http://ctdbase.org/, Score > 9) and Phenolyzer databases (http://phenolyzer.wglab.org/, Gene Intolerance Score > 0.9). Jvenn tool (http://jvenn.toulouse.inra.fr/app/example.html) was used for intersection analysis of the significantly highly expressed genes and NSCLC-related genes. In order to further screen the key factors, we analyzed the interaction relationship between genes through the STRING website (https://string-db.org/), and imported the interaction relationship network into the software Cytoscape 3.5.1, to analyze the nodes of the network by using the software's built-in tool NetworkAnalyzer, and their sort according to the node value (Degree) of genes. We analyzed the KM survival curve, ROC curve and gene risk of genes in lung cancer through the Sangerbox online tool (http://sangerbox.com/), set HR > 1, P Value < 0.05 as the risk assessment standard, where the area under the ROC curve AUC > 0.5 is the evaluation standard of survival risk models.

Study subjects
NSCLC tissues and adjacent normal tissues more than 5 cm away from the tumors were collected from 75 patients diagnosed with NSCLC at the First Affiliated Hospital of Zhengzhou University from 2009 to 2013[18]. None of the enrolled patients had received local or systemic treatment prior to the collection of clinical samples. One part of resected tissue samples were immediately stored in liquid nitrogen and the other part was fixed by immersion in 4% formalin, conventionally dehydrated, and embedded in paraffin. Classification of histological type and tumor-node-metastasis (TNM) stage followed the National Comprehensive Cancer Network (NCCN) guidelines[19]. All the patients had follow-up for 5 to 60 months. Survival analysis of those patients was performed using the Kaplan–Meier method. During the follow-up period, the death of patients or the last follow-up visit was considered as the end point, and the time interval between the date of operation and the date of patient death was defined as the overall survival (OS).

Immunohistochemistry
The paraffin-embedded tissues were cut into 4-μm-thick sections and dewaxed, followed by hydration. Immunohistochemistry staining was conducted in tissue sections using the primary antibody to PLOD3 (ab128698, 1:300) and secondary antibody to immunoglobulin G (IgG; ab150083, 1:100) (both purchased from Abcam Inc., Cambridge, UK). The percentage of positive cells was counted in five randomly-selected regions under microscope, which was semi-quantitatively graded. A percentage of positive cells less than 15% was graded as negative (−), 15-25% as (+), 25-50% as (++), 50-75% as (+++), and more than 75% as (++++)[20,21].

Cell culture
Four NSCLC cell lines including A549 and H1299 from (Cell bank of Chinese Academy of Sciences; http://www.cellbank.org.cn), Calu6 from Procell Life Science & Technology Co., Ltd. (Wuhan, China), and H520 from American type culture collection (ATCC, USA), as well as normal human bronchial epithelial cell line HBEC-3KT (ATCC) were used for this study. All cell lines were incubated in Dulbecco's modified Eagle's medium (DMEM) (12800017; Gibco, Carlsbad, California, USA) containing 10% fetal bovine serum (FBS; 26140079, Gibco) and 1% penicillin/streptomycin in an

incubator (BB15; Thermo Fisher Scientific, Massachusetts, USA) with 5% CO_2 and saturated humidity at 37 °C. With the medium renewed every 24 h, the cells were passaged every 72 h.

After cells were detached with 0.25% trypsin for 3 min, the reaction was terminated by culturing with DMEM containing 10% FBS. Subsequently, the cells were triturated into single-cell suspension and conventionally sub-cultured. Finally, cells at the logarithmic growth phase were collected to determine PLOD3 expression using the reverse transcription quantitative polymerase chain reaction (RT-qPCR), and the cell line with the highest expression of PLOD3 was selected for follow-up experiments.

Cell treatment
Cells were seeded into 6-well plates, cultured for 24 h, and then transfected with different plasmids using Lipofectamine2000 reagent (11668019, Thermo Fisher Scientific) upon reaching about 70% confluence. The plasmids used were sh-NC (nonsense negative control sequence), sh-PLOD3 (shRNA targeting PLOD3), oe-PKCδ (plasmid overexpressing PKCδ), sh-PLOD3 + oe-PKCδ, CDK1 + DMSO (plasmid overexpressing CDK1 and dimethyl sulfoxide, solvent of CDK1 kinase inhibitor), CDK1 + Purvalanol A (plasmid overexpressing CDK1 and CDK1 kinase inhibitor, Purvalanol A), oe-NC, oe-LIMD1 (plasmid overexpressing LIMD1), CDK1 + oe-LIMD1 (plasmid overexpressing CDK1 and LIMD1), oe-YAP1 (plasmid overexpressing YAP1) or oe-LIMD1 + oe-YAP1 (plasmid overexpressing LIMD1 and YAP1). The plasmid construction was accomplished by Shanghai Genechem Co., Ltd. (Shanghai, China). RT-qPCR was conducted to determine the silencing efficiency of shRNAs against PLOD3, including sh-PLOD3#1, sh-PLOD3#2, and sh-PLOD3#3, and the shRNA inducing the lowest expression of PLOD3 was selected for use in the following experiments.

RNA isolation and quantitation
Total RNA was extracted from tissues or cells using the TRIzol kit (Invitrogen, Carlsbad, CA, USA). Total RNA was reversely transcribed into complementary DNA (cDNA) using the reverse transcription kit (K1622, Beijing Reanta Biotechnology Co., Ltd., Beijing, China). Subsequently, real-time qPCR was performed on the ABI 7500 fluorescence quantitative PCR instrument (Applied Biosystems, Foster City, CA, USA) as per the instructions of the SYBR®Premix Ex Taq™ II kit (Takara, Kyoto, Japan). With glyceraldehyde 3-phosphate dehydrogenase (GAPDH) as an internal reference, the relative expression of target genes was calculated by means of relative quantification $2^{-\Delta\Delta Ct}$ method (Table S1) according to the following formula: $\Delta\Delta Ct = \Delta CT_{(experimental\ group)} - \Delta CT_{(control\ group)}$, $\Delta Ct = CT_{(target\ gene)} - CT_{(internal\ reference)}$[22].

Western blot analysis
Total protein was extracted from cells or tissues using pre-cooled radio-immunoprecipitation assay (RIPA) lysis buffer (R0010, Beijing Solarbio Science & Technology Co. Ltd., Beijing, China) containing phenylmethyl-sulfonyl fluoride (PMSF). The protein concentration was determined using a bicinchoninic acid (BCA) assay kit (20201ES76, Yeasen Company, Shanghai, China). After quantitation, the proteins were separated by polyacrylamide gel electrophoresis (PAGE) and transferred onto poly-vinylidene fluoride (PVDF) membranes (Millipore, Billerica, MA, USA) using the wet transferring method. The membrane was blocked with 5% bovine serum albumin (BSA) for 1 h at room temperature, and then incubated overnight at 4 °C with diluted rabbit primary antibodies against PLOD3 (ab128698, 1:1500), PKCδ (ab182126, 1:5000), caspase-3 (ab13847, 1:500), cleaved caspase-3 (ab32042, 1:500), CDK1 (ab131450, 1:800), p-CDK1 (ab133463, 1:1500), LIMD1 (ab225714, 1:5000), p-LIMD1 (#13245, 1:1000), YAP1 (ab52771, 1: 5000), p-YAP1 (ab62751, 1:2000), p53 (ab131442, 1:800), B-cell lymphoma 2 (Bcl-2) (ab182858, 1:2000), E-cadherin (ab40772, 1:10,000), Snail (ab180714, 1:1000), Fibronectin (ab2413, 1:2000), p-PERK (ab192591, 1:1000), PERK (sc-377400, 1:1000), eIF2α (#5324, 1:1000), p-eIF2α (ab32157, 1:1000), p-IRE1α (ab124945, 1:1000), IRE1α (ab37073, 1:1000), ATF6 (ab122897, 1:1000) and γH2AX (ab81299, 1:1000). The next day, the membrane was washed with Tris-buffered saline tween (TBST), and then incubated with horseradish peroxidase (HRP)-labeled secondary antibody, goat anti-rabbit IgG (ab6721, 1:5000) at room temperature for 1 h. The aforementioned antibodies were purchased from Abcam Inc. except the rabbit anti p-LIMD1 and eIF2α, which were purchased from Cell Signaling Technology (Beverly, MA, USA). After secondary treatment, the membrane was washed with TBST and then developed. With GAPDH (1:5000, 10494-1-AP, Proteintech Group, Chicago, IL, USA) as the internal reference, the protein bands were analyzed using Quantity One

v4.6.2 software, and the ratio of the gray values between the target band and GAPDH band was taken as the relative expression.

Fractionation of nuclear and cytoplasmic proteins

The collected undetected NSCLC cells were resuspended with 200 μL CEB-A buffer, oscillated for 15 s, and incubated on ice for 10 min. Then, 11 μL of cytoplasmic protein extraction buffer was added, whereupon the cells were oscillated for 5 s and then placed on ice for 1 min. After centrifugation at 16,000 g at 4 °C for 5 min, the supernatant (cytoplasmic fraction) was immediately collected into a new Eppendorf (EP) tube and placed on ice. The pellet was resuspended with 100 μL nucleus protein extraction buffer, oscillated for 15 s, and incubated on ice for 10 min. The suspension was again vortexed for 15 s and incubated on ice for 10 min, thus four times in total. After centrifugation at 16,000 g at 4 °C for 10 min, the supernatant (nuclear fraction) was immediately collected into a new EP tube and placed on ice. Western blot analysis was applied to measure the expression of relevant proteins in the nuclear and cytoplasmic fractions.

Detection of caspase-3 activity

A549 cells at logarithmic growth phase after lentivirus infection were collected, digested, and counted. The cells were seeded into 6-well plates at a density of 1×10^6 cells/mL with 2 mL of medium added per well, and cultured overnight until attaining 80% confluence. Next, the cells were transfected with caspase-3-promoter luciferase reporter vector with dual luciferase gene reporter system. After 48 h of culture, cells were lysed by RIPA lysis buffer (R0010, Beijing Solarbio Science & Technology Co. Ltd.). The supernatant was collected and assayed for the activity of caspase-3 according to the instructions of caspase-3 activity detection kit (ab39383, Abcam Inc.), and for protein concentration by the BCA method.

Immunofluorescence staining

Cells were seeded in a 6-well plate and treated with tert-butyl hydrogen peroxide (TBHP) (100 μmol/L) for 2 h. The cells were fixed in 2% freshly-prepared paraformaldehyde. Afterwards, the cells were treated with 0.2–0.5% TritonX-100/PBS, and then incubated at 4 °C overnight with the primary antibodies against PLOD3 (ab89263, 1:100), PKCδ (ab182126, 1:200), cleaved caspase-3 (ab32042, 1:200), p-CDK1 (ab133463, 1:1500), YAP1 (ab52771, 1:300), and p-YAP1 (ab62751, 1:2000). The next day, the cells were incubated for 1 h at 37 °C with the secondary antibodies labeled by fluorescein isothiocyanate (FITC) green fluorescence (ab6717, 1:2000) and by Cy3 ® red fluorescence (ab6939, 1:2000). All the antibodies above were purchased from Abcam Inc. Then, cells were rinsed by phosphate-buffered saline (PBS), and stained with Hoechst reagent for 10 min, following by PBS washing and mounting. After that, laser confocal microscope (CV1000, YOKOGAWA, Shanghai, China) was applied for observation and photographing. The cells positive for PLOD3, PKCδ, cleaved caspase-3, p-CDK1, and YAP1 were counted and calculated as the percentages of positive cells. The positive expression of PLOD3, YAP1, and p-YAP1 was indicated by red fluorescence and that of PKCδ, cleaved caspase-3, p-LIMD1, and p-CDK1 was indicated by green fluorescence.

Cell Counting Kit-8 (CCK-8) assay

The cell viability was detected using CCK-8 kit (CA1210-100, Beijing Solarbio Science & Technology Co., Ltd.). The cells at the exponential growth phase were seeded in 96-well plates with 5×10^3 cells per well and cultured for 3 days. On days 1, 2, and 3, cells in each well were incubated with 10 μL CCK-8 solution for 2 h. Subsequently, the optical density (OD) value at 450 nm in each well was measured by a microplate reader (BIO-RAD 680, Bio-Rad Laboratories, Hercules, CA, USA). The cell growth curve was then plotted.

Colony formation assay

The cells at logarithmic growth phase were collected and resuspended by DMEM. Then, the cell suspension was seeded in a 6-well plate with 2×10^2 cells per well, and three duplicated wells were set for each group. Next, cells were placed to stand on a super clean bench for 20 min and transferred to the incubator. Fourteen days later, the cells were fixed with 10% paraformaldehyde for 5 min, stained by 1% crystal violet for 10 min, and fully rinsed by distilled water. Subsequently, cells were observed, counted (clone containing more than 50 cells), and photographed under a biological inverted microscope (MI12, MSHOT, Guangzhou, China). The colony formation rate = number of formed clones/number of inoculated cells × 100%.

Flow cytometry

For detection of cell cycle, cells were centrifuged 48 h after transfection and the supernatant was discarded. After resuspension in PBS, the cell concentration was adjusted to about 1×10^5 cells/mL. Then, cells were fixed for 1 h at 4 °C by 1 mL of 75% cold ethanol, centrifuged, and washed with PBS. The fixed cells were then incubated with 100 μL RNase A at 37 °C for 30 min, and stained with 400 μL propidium iodide (PI) (Sigma-Aldrich Chemical Company, St Louis, MO, USA) at 4 °C for 30 min in the dark. Finally, a flow cytometer was employed to analyze the cell cycle at an excitation wavelength of 488 nm.

For detection of cell apoptosis, 48 h after transfection cells were detached with trypsin in the absence of ethylenediamine tetraacetic acid (EDTA), centrifuged in a flow cannula, and the supernatant discarded. Then, the pellets were washed with cold PBS and re-centrifuged. Next, the Annexin-V-FITC/PI dye liquor was prepared by mixing Annexin-V-FITC, PI, and hydroxyethyl piperazine ethane-sulfonic acid (HEPES) at the volume ratio of 1:2:50, following the instructions of Annexin-V-FITC cell apoptosis detection kit (Sigma-Aldrich Chemical Company, St Louis, MO, USA). Samples of 1×10^6 cells were incubated with 100 μL dye liquor at room temperature for 15 min. Subsequently, cells were added with 1 mL HEPES buffer, oscillated, and mixed. At the excitation wavelength of 488 nm, the bandpass filters of 525 nm and of 620 nm were used to measure the FITC fluorescence and PI fluorescence for cell apoptosis detection.

Xenograft tumor model in nude mice

Twelve male-specific pathogen-free (SPF) BALB/c nude mice (aged 4 weeks, weighing 20-22 g) (Shanghai SLAC Laboratory Animal Co., Ltd., Shanghai, China) were used for this study. Cells stably transfected with sh-NC or sh-PLOD3 were prepared. The cells were collected, washed with PBS, and triturated into single-cell suspension. A total of 2×10^6 cells were resuspended by 50 μL normal saline, mixed with 50 μL Matrigel Matrix (1:1) and then inoculated into the armpit of the mice, assigned randomly to groups receiving cells stably expressing sh-NC or sh-PLOD3 (six mice each). Subsequently, the mice were euthanized by 40 mg/kg pentobarbital on the 7th, 14th, 21st, and 28th days, and then the transplanted tumors were excised, followed by measurement of tumor weight and volume.

TdT-mediated dUTP nick-end labeling (TUNEL) assay

The tumor tissues were fixed overnight with 4% paraformaldehyde and embedded in paraffin, and then sectioned at a thickness of 5 μm. Five sections of the mouse brain cortex tissues were deparaffinized, added with 1% 50 μL of proteinase K dilution solution, and incubated at 37 °C for 30 min. Next, the sections were added with 0.3% H_2O_2/methanol solution to eliminate endogenous POD activity, incubated at 37 °C room temperature for 30 min, and added with TUNEL reaction solution dropwise, followed by incubation in a humid box at 37 °C for 1 h in the dark. The sections were added with 50 μL Converter-POD for incubation in the humid box at 37 °C for 30 min, and then developed by 2% diaminobenzidine (DAB), followed by incubation at room temperature for 15 min. After brown cell nuclei were observed under the microscope, cells were added with distilled water to terminate the reaction, followed by counterstaining of hematoxylin and dehydration with 50, 70, 90, and 100% gradient ethanol. After clearing with xylene, the sections were sealed with neutral gum and observed under an optical microscope in ten randomly selected fields. The cells with brown nucleus were apoptosis-positive cells, and the cells with blue nucleus were normal cells.

Immunohistochemistry

The tumor tissues were fixed into 4% paraformaldehyde phosphate buffer solution for 12 h, followed by conventional xylene dewaxing and gradient alcohol hydration (absolute ethanol, 95% ethanol, 75% ethanol for 3 min each). The sections were placed in 0.01 M citrate buffer and boiled for 15–20 min, cooled to room temperature, added with goat serum blocking solution, and placed at room temperature for 20 min, followed by the removal of the excess liquid. The sections were added with 50 μL of primary antibody against proliferating cell nuclear antigen (PCNA; ab92552, 1:200, Abcam), then 50 μL of secondary antibody goat anti-rabbit IgG (ab6728, 1: 1000, Abcam), and left at room temperature for 1 h. After washing with PBS, sections were incubated with streptavidin-peroxidase added dropwise for 30 min at 37 °C, followed by DAB development for 5-10 min and addition of water to terminate the reaction. Sections were then hematoxylin counterstained for 2 min, and differentiated with hydrochloric acid and alcohol, washed with tap water for 10

min, routinely dehydrated, cleared, and mounted, and observed under an inverted microscope.

Statistical analysis

All data were processed by SPSS 21.0 statistical software (IBM Corp. Armonk, NY, USA). Measurement data were summarized by mean ± standard deviation. Data with normal distribution and homogeneity of variance between two groups were compared using paired t-test (paired data) or unpaired t-test (unpaired data). Data among multiple groups were tested by one-way analysis of variance (ANOVA) with Tukey's post hoc test. Data at different time points were compared using repeated measures ANOVA with Bonferroni post hoc test. Correlation analysis was performed by Pearson's correlation coefficient. Survival rate of patients was analyzed using the Kaplan–Meier method and compared using the Log-rank test. $p < 0.05$ was considered as statistically significant.

RESULTS

High expression of PLOD3 was observed in NSCLC tissues and cells and is correlated with poor survival of NSCLC patients

Differential analysis on the NSCLC-related GSE19188 dataset yielded 4674 significantly highly expressed genes in NSCLC. The CTD and Phenolyzer databases predicted 9141 and 1285 NSCLC-related genes, respectively. Intersection analysis of the significantly highly expressed genes and NSCLC-related genes revealed 170 candidate genes (Fig. 1A). To further screen the key factors, we analyzed the interaction relationship among 170 genes using the STRING website and constructed a gene interaction network by the Cytoscape 3.5.1 software (Fig. 1B). According to the Degree value of genes, 32 genes were at the core of the network (Degree ≥8). The expression heat map of 32 candidate genes in the NSCLC-related dataset was obtained by R language (Fig. 1C). According to the heat map, we found that CDH1, COL2A1 and PLOD3 genes ranked the top in p-value ranking. The gene PLOD3 was identified as a high-risk gene in lung cancer by the Sangerbox online tool (Fig. 1D), and the Kaplan–Meier survival curve and ROC curve of PLOD3 (area under curve AUC > 0.5) were obtained (Fig. 1E). The results showed that the high expression of PLOD3 led to a significant decrease in the survival rate of NSCLC patients.

High expression of PLOD3 has been evidenced in several human malignancies, including lung cancer, liver cancer and glioma, in which the promotion of growth, invasion, and migration of tumor cells has suggested that PLOD3 acts as an oncogene[5,7,23,24]. RT-qPCR data revealed that the expression of PLOD3 was higher in the NSCLC tissues than in adjacent normal tissues (Fig. 1F). Immunohistochemistry displayed that the PLOD3 was localized both in the cytoplasm and nucleus. The positive rate of PLOD3 was much higher in NSCLC tissues than in adjacent normal tissues [81.3% (61/75) vs. 18.7% (14/75), $p < 0.05$] (Fig. 1G). Moreover, Western blot analysis revealed that the protein expression of PLOD3 was much higher in NSCLC tissues than in adjacent normal tissues (Fig. 1H, Supplementary Fig. 1A). Therefore, we confirm that PLOD3 was highly expressed in NSCLC tissues.

Correlation analysis of the PLOD3 expression with clinicopathological characteristics of 75 NSCLC patients displayed that there were more NSCLC patients with high expression of PLOD3 than th than with low expression of PLOD3 (all $p < 0.05$). PLOD3 expression exhibited no correlation with the gender, age, tumor type, and smoking history, but was related to advanced clinical stage, TNM classification, and N staging of NSCLC patients (Table S2). The Kaplan–Meier curve displayed that patients with high PLOD expression had higher OS than patients with low PLOD3 expression (all $p < 0.05$) (Fig. 1I). Hence, high PLOD3 expression was correlated with cancer progression and poor survival of NSCLC patients.

RT-qPCR data further revealed that, in comparison with HBEC-3KT cells, the four NSCLC cell lines (A549, H1299, Calu6, and H520) all showed higher expression of PLOD3. A549 cells showed the highest expression of PLOD3 (Fig. 1J) and were thus selected for subsequent experiments.

Silencing of PLOD3 induces the generation of PKCδ catalytic fragment cleaved by caspase-3

A previous study has reported that PLOD3 could regulate the PKCδ signaling pathway[7]. Protein kinase C δ (PKCδ), a member of the PKC family, has been recognized as a tumor promoter or suppressor with differing specificities in various tumor types, and can furthermore regulate the balance between tumor cell death and proliferation. Studies in PKCδ$^{-/-}$ mice have confirmed the pro-apoptotic role for this kinase in response to DNA damage, and as a tumor promoter role in some oncogenic contexts. Because apoptosis is an important anti-tumor mechanism, PKCδ was initially proposed to act as a tumor suppressor[8,25,26]. Accumulating studies have proved that the PKCδ signaling pathway is indeed a tumor-suppressive pathway, in which cleaved PKCδ is a catalytically active fragment[9,10,27]. Therefore, we sought to investigate whether PLOD3 could mediate the PKCδ signaling pathway in NSCLC. To answer this question, we silenced PLOD3 in A549 cells by three independent shRNAs, i.e., sh-PLOD3#1, sh-PLOD3#2, and sh-PLOD3#3. As determined by RT-qPCR, the lowest expression of PLOD3 was found after transfection with sh-PLOD3#2 among the three variants (all $p < 0.05$) (Fig. 2A), and we thus selected sh-PLOD3#2 for use in following studies.

Western blot analysis provided evidence that the protein expression of PLOD3 and PKCδ was inhibited in cells transfected with sh-PLOD3, accompanied with induction of cleaved PKCδ and increased expression of cleaved ecapase-3 protein, whereas the expression of total caspase-3 protein was unaffected (Fig. 2B, Supplementary Fig. 1B). Immunofluorescence staining displayed that PLOD3 (red fluorescence) was expressed both in the nucleus and cytoplasm, while PKCδ and cleaved caspase-3 (green fluorescence) were mainly expressed in the nucleus. Knockdown of PLOD3 suppressed the protein expression of PKCδ, but elevated that of cleaved caspase-3 (Fig. 2C).

Furthermore, the nuclear and cytoplasmic fractions and Western blot analysis revealed that PLOD3 was expressed both in nucleus and cytoplasm, with a larger proportion in the nucleus. Besides, PKCδ and caspase-3 were expressed both in the nucleus and cytoplasm, while cleaved PKCδ and cleaved caspase-3 were mainly expressed in the nucleus. Furthermore, knockdown of PLOD3 reduced the expression of PKCδ, but elevated that of cleaved caspase-3 (Fig. 2C) and induced the activation of caspase-3 (Fig. 2D). Western blot analysis indicated that A549 cells with knockdown of PLOD3 exhibited an increase in the expression of ER stress protein, including cleaved ATF6 expression and phosphorylation levels of PERK and IRE1α, as well as the expression of the DNA damage marker γH2AX (Fig. 2E, Supplementary Fig. 1C). All the above results support the conclusion that PLOD3 regulates the PKCδ signaling pathway through mediating the activation of caspase-3. Silenced PLOD3 reduced the expression of PKCδ, and induced activated caspase-3, which triggered generation of cleaved PKCδ.

Silencing of PLOD3 suppresses proliferation and progression of NSCLC by upregulating cleaved PKCδ and phosphorylating CDK1

CDK1 is highly expressed in NSCLC, in which it promotes proliferation, migration, invasion, and mitosis. The dephosphorylated CDK1 exerts kinase activity, which then promotes the cell proliferation. Cleaved PKCδ could promote the phosphorylation level of CDK1, and thus inactivate CDK1 to suppress cell proliferation[28–30]. Therefore, we decided to explore whether phosphorylation and activity of CDK1 could be regulated by PKCδ in NSCLC.
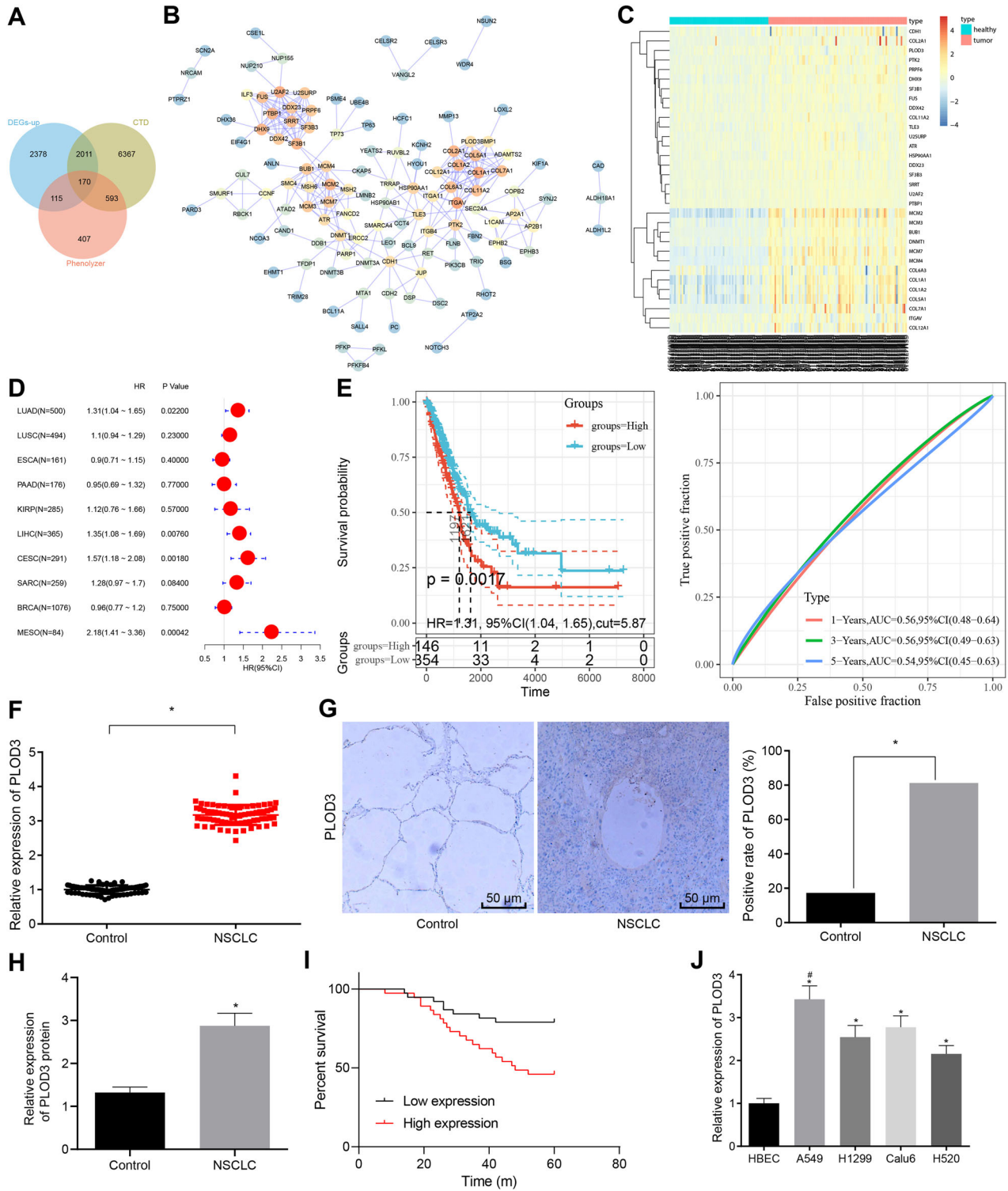
Fig. 1 PLOD3 is highly expressed in NSCLC tissues and cells. A Venn diagram of the intersection of differentially expressed genes with significantly high expression in NSCLC and NSCLC related genes in the CTD and Phenolyzer databases; **B** Interaction relationship network diagram of candidate genes, dot color scale from blue to orange, where the degree values of genes is from small to large; **C** Heat map of candidate gene expression in NSCLC datasets; **D** Risk score of PLOD3 gene in different tumors; **E** KM survival curve and ROC curve of PLOD3; **F** The mRNA expression of PLOD3 in the NSCLC tissues and adjacent normal tissues determined by RT-qPCR. **G** The positive expression of PLOD3 in the NSCLC tissues and adjacent normal tissues detected by immunohistochemistry. **H** The protein expression of PLOD3 in the NSCLC tissues and adjacent normal tissues measured by Western blot analysis. **I** The OS of NSCLC patients analyzed by Kaplan–Meier method. **J** The relative PLOD3 mRNA expression in NSCLC cell lines (A549, H1299, Calu6, and H520) and normal HBEC-3KT cell line determined by RT-qPCR. *$p < 0.05$, compared with adjacent normal tissues or normal HBEC cell line; #, the cell line with the highest expression of PLOD3. The results above were measurement data, which were expressed as mean ± standard deviation from three independent experiments. Data between two groups were analyzed by t-test and data among multiple groups were analyzed by one-way ANOVA.
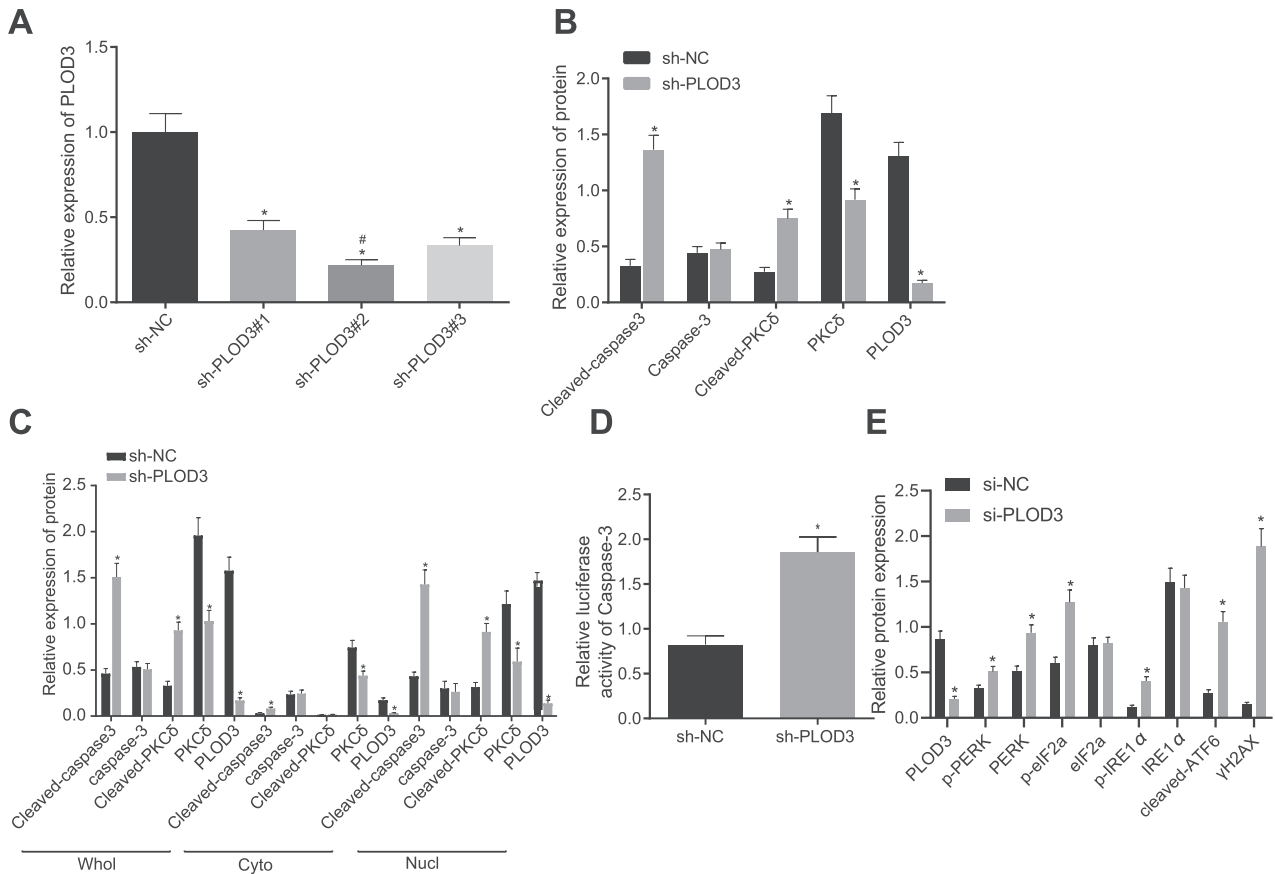
Fig. 2 Loss of PLOD3 contributes to the generation of an active catalytic fragment cleaved PKCδ cleaved by caspase-3. A The silencing efficiency of shRNAs targeting PLOD3 determined by RT-qPCR. **B** The protein expression of PLOD3, PKCδ, cleaved PKCδ, caspase-3 and cleaved caspase-3 in the A549 cells transfected with sh-PLOD3 measured by Western blot analysis. **C** The protein expression of PLOD3, PKCδ, and cleaved caspase-3 in the A549 cells transfected with sh-PLOD3 determined by immunofluorescence staining. **D** The caspase-3 activity in the cells transfected with sh-PLOD3. **E** The protein expression of PLOD3, cleaved ATF6, and DNA damage marker γH2AX, as well as phosphorylation levels of PERK, eIF2a, and IRE1α in A549 cells transfected with sh-PLOD3 measured by Western blot analysis. *$p < 0.05$, compared with cells transfected with sh-NC; #, the highest silencing efficiency of shRNA against PLOD3. The results above were measurement data, which were expressed as mean ± standard deviation from three independent experiments. Data between two groups were analyzed by unpaired t-test and data among multiple groups were analyzed by one-way ANOVA, with Tukey's post hoc test.

RT-qPCR showed that the mRNA expression of CDK1 was much higher in 75 cases of NSCLC tissues than in adjacent normal tissues (Fig. 3A). Also, Western blot analysis displayed that the NSCLC tissues exhibited much higher protein expression of CDK1, but much lower CDK1 phosphorylation levels than the adjacent normal tissues (Fig. 3B). These findings suggested aberrant high expression of CDK1 but inhibited phosphorylation levels of CDK1 in NSCLC.

To explore the regulatory effect of PLOD3/PKCδ/CDK1 on NSCLC, the A549 cells were transfected with sh-NC, sh-PLOD3, oe-NC, oe-PKCδ, or co-transfected with sh-PLOD3 and oe-PKCδ. No obvious change in mRNA expression of CDK1 was observed in the cells after transfection, as shown by RT-qPCR (Fig. 3C). The results of Western blot analysis displayed that knockdown of PLOD3 elevated the protein expression of cleaved PKCδ and enhanced phosphorylation levels of CDK1. Similarly, overexpression of PKCδ upregulated the protein expression of cleaved PKCδ and increased the phosphorylation levels of CDK1, the effect of which could be more evident following further silencing of PLOD3 (Fig. 3D). These results suggest that PLOD3 inhibits the phosphorylation of CDK1 kinase by inhibiting the PKCδ signaling pathway.

As depicted by immunofluorescence staining, PKCδ (red fluorescence) was expressed in nucleus and to a lesser extent in cytoplasm, where p-CDK1 (green fluorescence) was expressed exclusively in the nucleus. Knockdown of PLOD3 reduced protein expression of PKCδ but elevated phosphorylation levels of CDK1. Overexpression of PKCδ significantly suppressed phosphorylation levels of CDK1 but had no effect on the PLOD3 expression. However, knockdown of PLOD3 in part reversed the suppressed phosphorylation levels of CDK1 mediated by overexpression of PKCδ (Fig. 3E, Supplementary Fig. 2A).

The results of the CCK-8 assay, colony formation experiment, and flow cytometry revealed that knockdown of PLOD3 reduced the proliferation of A549 cells, weakened the colony formation, prolonged the G0/G1 phase of the cells, shortened the S and G2/M phases, and promoted the apoptosis of A549 cells. The overexpression of PKCδ resulted in increased proliferation of A549 cells, enhanced colony formation, shortened G0/G1 phases, prolonged S and G2/M phases, and inhibited A549 cell apoptosis (Fig. 3F–I, Supplementary Fig. 3A). Therefore, we supposed that silenced PLOD3 upregulated cleaved PKCδ and promoted CDK1 phosphorylation inactivation, thus suppressing cell proliferation and promoting cell apoptosis of NSCLC. PLOD3 is an inhibitor of the PKCδ signaling pathway activation. Overexpression of PLOD3 inhibited PKCδ cleavage and reduced the expression of cleaved PKCδ. Since cleaved PKCδ can promote the phosphorylation of CDK1, any decrease of cleaved PKCδ would inhibit the phosphorylation of CDK1, thus promoting cell proliferation and inhibiting cell apoptosis. Therefore, the highly expressed PLOD3 induces the further development and deterioration of NSCLC.
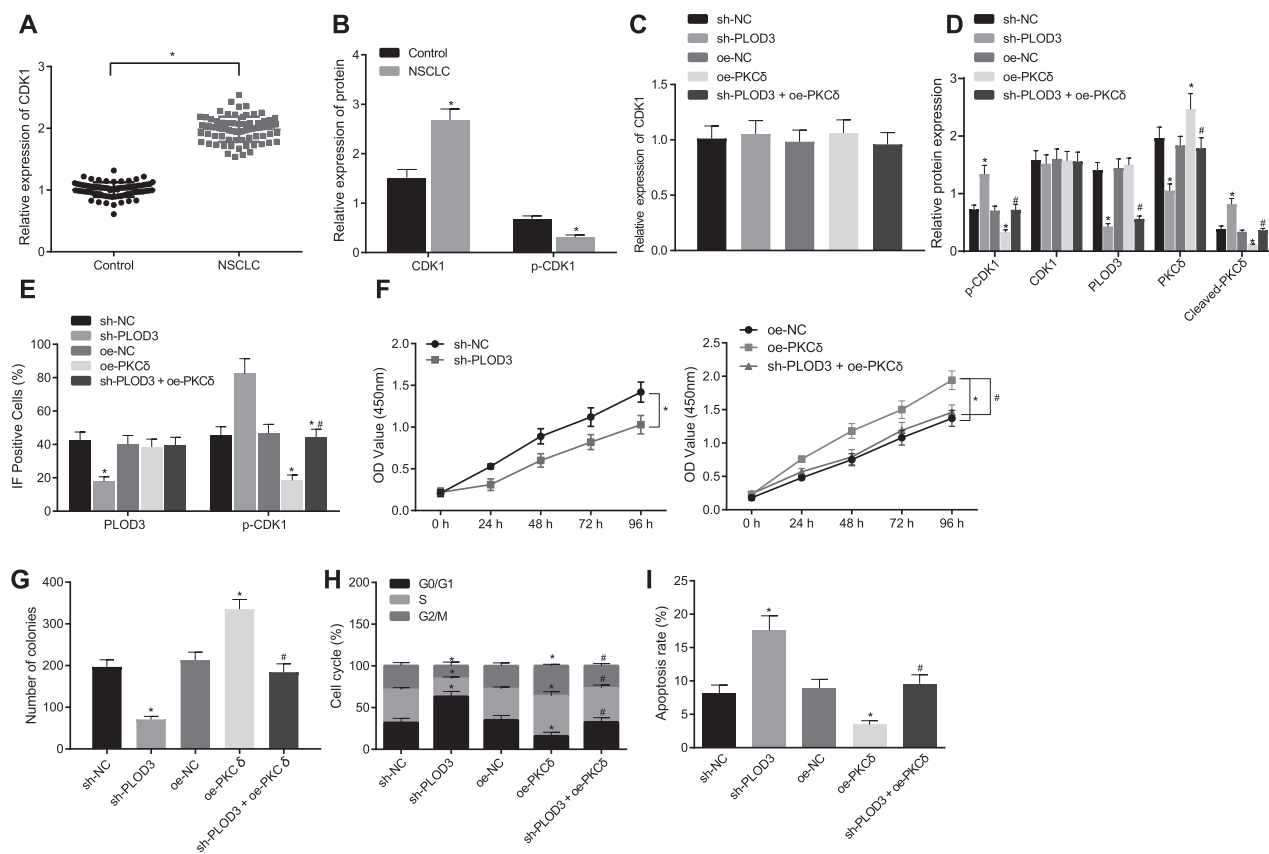
Fig. 3 Knockdown of PLOD3 prevents NSCLC progression through upregulation of cleaved PKCδ and CDK1 phosphorylation. A The mRNA expression of CDK1 in NSCLC tissues and adjacent normal tissues determined by RT-qPCR. **B** The protein expression of CDK1 and phosphorylation levels of CDK1 in NSCLC tissues and adjacent normal tissues measured by Western blot analysis. The cells used for the following assays were transfected with sh-NC, sh-PLOD3, oe-NC and oe-PKCδ or co-transfected with sh-PLOD3 and oe-PKCδ. **C** The mRNA expression of CDK1 in the transfected cells determined by RT-qPCR. **D** The protein expression of cleaved PKCδ and CDK1 and phosphorylation levels of CDK1 in the transfected cells detected by Western blot analysis. **E** The protein expression of PLOD3 and phosphorylation levels of CDK1 in the transfected cells examined by immunofluorescence staining. **F** The viability of the transfected cells detected by CCK-8 assay. **G** The colony formation of the transfected cells determined by colony formation assay. **H, I** The cell cycle entry and cell apoptosis after transfection examined by flow cytometry. *$p < 0.05$, compared with cells transfected with sh-NC or oe-NC; #$p < 0.05$, compared with cells transfected with oe-PKCδ. The results above were measurement data, which were expressed as mean ± standard deviation from three independent experiments. Data between two groups were analyzed by unpaired t-test and data among multiple groups were analyzed by one-way ANOVA, with Tukey's post hoc test. Data among multiple groups at different time points were compared by repeated measures ANOVA with Bonferroni's post hoc test.

Phosphorylation of CDK1 promotes phosphorylation of LIMD1 and inhibits the proliferation and progression of NSCLC

CDK1 is an upstream kinase that can phosphorylate LIMD1 among other substrates. Previous studies have found that LIMD1 acts as a tumor suppressor in various cancers, and participates in the regulation of cellular functions by controlling mitosis[12,14]. Thus, the functional role of LIMD1 in NSCLC was pursued for detailed scrutiny. Initially, RT-qPCR showed that LIMD1 exhibited lower mRNA expression in NSCLC tissues than in adjacent normal tissues (Fig. 4A). The protein expression of LIMD1 and phosphorylation levels of LIMD1 were much lower in NSCLC tissues than in adjacent normal tissues, as detected by Western blot analysis (Fig. 4B). Besides, Pearson's correlation coefficient (Fig. 4C) displayed that phosphorylation levels of CDK1 were positively correlated with those of LIMD1 ($p < 0.001$), suggesting that CDK1 phosphorylation might promote LIMD1 phosphorylation.

As a crucial oncogene, Bcl-2 promotes cancer cell survival by inhibiting apoptosis through the inactivation of proapoptotic proteins[31]. Fibronectin, a class of high-molecular-weight adhesive glycoproteins, exerts a pivotal function on ECM function because of its high abundance and its specific interactions with cellular components[32]. Expression of Snail1 in epithelial cells is reported to

trigger an epithelial-mesenchymal transition[33]. To explore the regulatory role of pKCδ/CDK1/LIMD1 in NSCLC, the A549 cells were transfected with oe-NC, oe-LIMD1, or co-transfected with oe-CKD1 and oe-LIMD1, or Purvalanol A, with DMSO treatment used as control. The results of RT-qPCR and Western blot analysis displayed that, compared with cells transfected with empty vector, overexpression of CDK1 and DMSO induced conspicuously increased expression of CDK1, Bcl-2, Snail, and Fironectin, but markedly enhanced phosphorylation levels of CDK1 and LIMD1 and reduced expression of p53 and E-cadherin, without significantly altering LIMD1 expression. The inhibition of CDK1 kinase activity by Purvalanol A partially rescued the changes in the above factors induced by overexpression of CDK1, accompanied by insignificant differences in LIMD1 expression, suggesting that phosphorylation of CDK1 is critical for the phosphorylation of LIMD1 and that CDK1 is the upstream activating molecule of LIMD1. On the other hand, transfection with oe-LIMD1 caused no marked changes in the expression of CDK1 and phosphorylation levels of CDK1, elevated the expression of LIMD1, p53 and E-cadherin, and phosphorylation levels of LIMD1, while reducing the expression of Bcl-2, Snail, and Fibronectin. The cells co-transfected with oe-CDK1 and oe-LIMD1 exhibited markedly increased expression of CDK1 and LIMD1 and
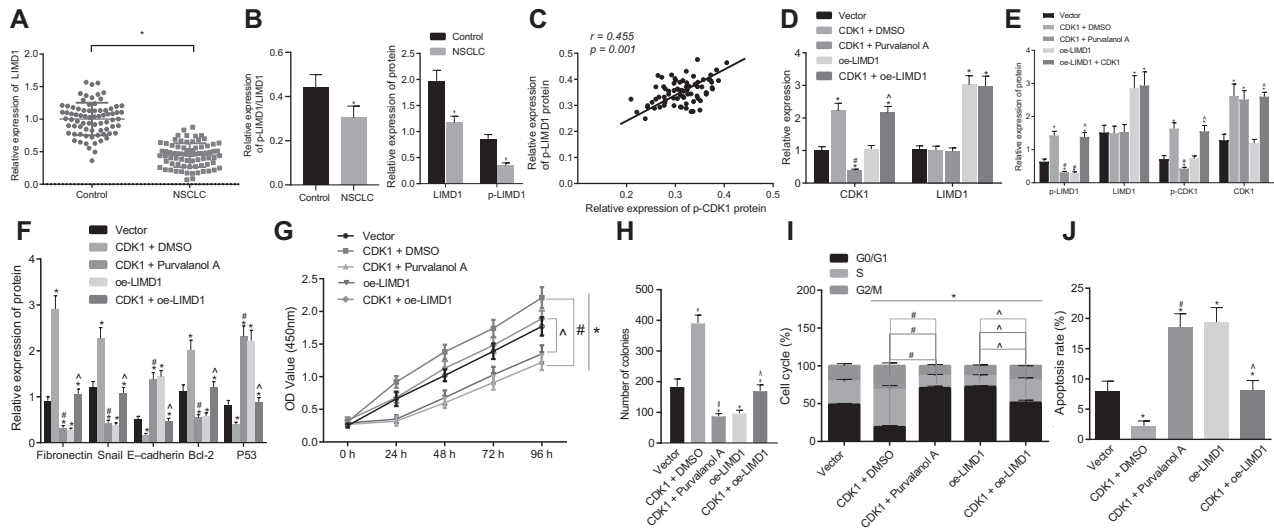
Fig. 4 CDK1 phosphorylation suppresses cell proliferation but enhances cell apoptosis of NSCLC by regulating LIMD1 phosphorylation.
A The mRNA expression of LIMD1 in NSCLC tissues and adjacent normal tissues determined by RT-qPCR. **B** The protein expression of LIMD1 and phosphorylation levels of LIMD1 protein in NSCLC tissues and adjacent normal tissues examined by Western blot analysis. The cells used for following detections were transfected with empty vector, oe-LIMD1, CDK1, or co-transfected with oe-LIMD1 and CDK1 vector, and also treated with Purvalanol A and DMSO in the presence of CDK1. **C** The correlation analysis of CDK1 phosphorylation and LIMD1 phosphorylation; Immunofluorescence staining of phosphorylation levels of CDK1 and LIMD1 after PLOD3 silencing (sh-PLOD3) on A549 cells. **D** The mRNA expression of CDK1 and LIMD1 in the cells following treatments determined by RT-qPCR. **E** The protein expression of CDK1 and LIMD1, as well as phosphorylation levels of CDK1 and LIMD1 in cells measured by Western blot analysis. **F** The protein expression of p53, Bcl-2, E-cadherin, Snail, and Fibronectin in cells examined by Western blot analysis. **G** The cell viability following treatments detected by CCK-8 assay. **H** The colony formation of the cells following treatments. **I, J** The cell cycle entry and cell apoptosis following treatments examined by flow cytometry. $*p < 0.05$, compared with cells transfected with empty vector; $\#p < 0.05$, compared with cells treated with both CDK1 vector and DMSO; $\wedge p < 0.05$, compared with cells transfected with oe-LIMD1. The results above were measurement data, which were expressed as mean ± standard deviation from three independent experiments. Data between two groups were analyzed by unpaired t-test and data among multiple groups were analyzed by one-way ANOVA with Tukey's post hoc test. Pearson's correlation coefficient was employed to analyze the correlation between CDK1 phosphorylation and LIMD1 phosphorylation. Data among multiple groups at different time points were compared by repeated-measures ANOVA with Bonferroni's post hoc test.

significantly decreased phosphorylation levels of CDK1, but had no pronounced difference in the phosphorylation levels of LIMD1, or the expression of p53, Bcl-2, E-cadherin, Snail, and Fibronectin as compared to cells transfected with empty vector (Fig. 4D–F, Supplementary Fig. 1D).

In the presence of CDK1, the treatment with Purvalanol A markedly decreased the expression of CDK1, Bcl-2, Snail, and Fibronectin, but enhanced phosphorylation levels of CDK1 and LIMD1, and expression of p53 and E-cadherin, while having no effect on the LIMD1 expression (Fig. 4D–F, Supplementary Fig. 3B). Relative to cells transfected with oe-LIMD1, cells co-transfected with both CDK1 vector and oe-LIMD1 showed remarkably increased expression of CDK1, Bcl-2, Snail and Fibronectin, markedly inhibited phosphorylation levels of CDK1, and reduced expression of p53 and E-cadherin and phosphorylation levels of LIMD1, along with the unaffected LIMD1 phosphorylation levels (Fig. 4D–F, Supplementary Fig. 3B). These results imply that LIMD1 phosphorylation could be induced by upregulated CDK1 phosphorylation, and that the kinase phosphorylation of CDK1 is critical for the phosphorylation of downstream LIMD1, thus indicating a signal cascade between CDK1 and LIMD1.

Results of the CCK-8 assay, colony formation assay, and flow cytometry found that overexpression of CDK1 increased the proliferation of A549 cells, and colony formation, shortened G0/G1 phase, prolonged S and G2/M phases, and reduced apoptosis; downregulate CDK1 or over-expression LIMD1 leads to the reduction of A549 cell proliferation, weakening of colony formation, prolongation of G0/G1 phase, shortening of S, G2/M phase, and increase of apoptosis. Finally, overexpression of LIMD1 can reverse the effect of overexpression of CDK1 on cell proliferation, colony formation, cell cycle, and apoptosis (Fig. 4G–J). These findings together suggest that

upregulated CDK1 phosphorylation level promotes LIMD1 phosphorylation, thus inhibiting cell proliferation and promote cell apoptosis and suppress the proliferation and progression of NSCLC.

LIMD1 phosphorylation downregulates YAP1 and alleviates the progression of NSCLC

YAP1 is one of the downstream factors of LIMD1[34–36], and acts as a tumor suppressor in NSCLC[16,37–40]. Thus, YAP1 is hyperactive in NSCLC, and the nuclear translocation of hyperactive YAP1 activates cell proliferation and then promotes NSCLC development. RT-qPCR and Western blot analysis showed that the expression of YAP1 was much higher in NSCLC tissues than in adjacent normal tissues (Fig. 5A, B). Also, the Pearson's correlation coefficient revealed that LIMD1 phosphorylation level was negatively correlated with YAP1 expression (Fig. 5C).

To investigate how YAP1 affected the progression of NSCLC, the A549 cells were transfected with oe-NC, oe-LIMD1, oe-YAP1 or co-transfected with oe-LIMD1 and oe-YAP1. RT-qPCR and Western blot analysis revealed that overexpression of LIMD1 promoted the phosphorylation levels of LIMD1, and elevated the expression of p53 and E-cadherin, but reduced the expression of YAP1, Bcl-2, Snail and Fibronectin as well as phosphorylation levels of YAP1. Overexpressed YAP1 had no effect on the expression of LIMD1 and phosphorylation levels of LIMD1, but reduced the expression of p53 and E-cadherin, and promoted YAP1 phosphorylation levels and elevated the expression of Bcl-2, Snail, and Fibronectin. Compared with overexpression of YAP1, overexpression of LIMD1 promoted LIMD1 phosphorylation levels but repressed phosphorylation levels of YAP1 and expression of YAP1, and additionally promoted the expression of p53 and E-cadherin, and reduced the expression of Bcl-2, Snail and Fibronectin (Fig. 5D–F).
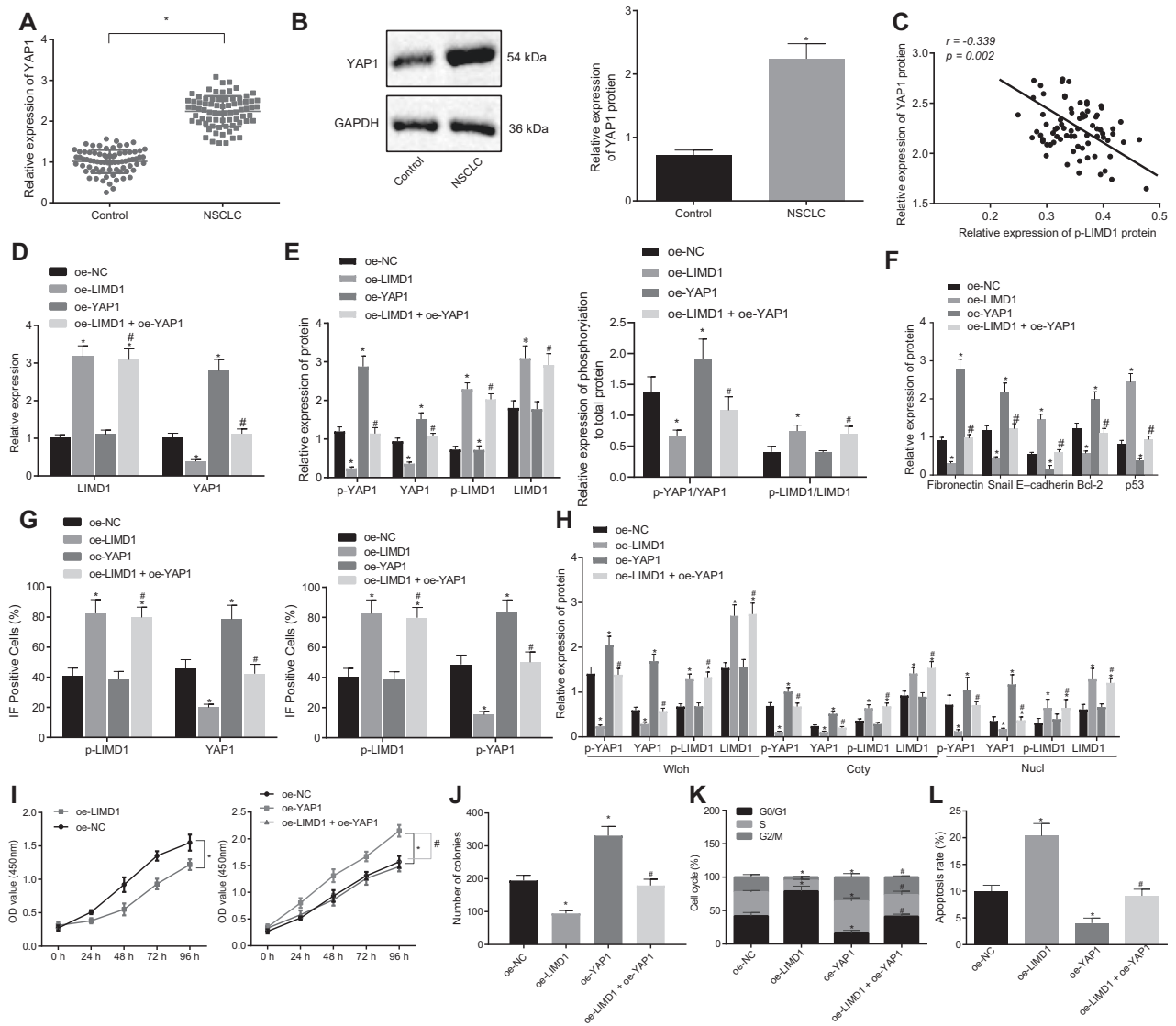
Fig. 5 LIMD1 phosphorylation reduces YAP1 expression and its nuclear translocation, thus suppressing the progression of NSCLC in vitro. A The mRNA expression of YAP1 in NSCLC tissues and adjacent normal tissues determined by RT-qPCR. **B** The protein expression of YAP1 in NSCLC tissues and adjacent normal tissues examined by Western blot analysis. The cells used for following detections were transfected with plasmids oe-NC, oe-LIMD1, oe-YAP1 or co-transfected with oe-LIMD1 and oe-YAP1. **C** The correlation analysis of phosphorylation levels of LIMD1 and phosphorylation levels of YAP1. **D** The mRNA expression of LIMD1 and YAAP1 in cells determined by RT-qPCR. **E** The protein expression of LIMD1 and YAP1, as well as phosphorylation levels of LIMD1 and YAP1 in cells detected by Western blot analysis. **F** The expression of p53, Bcl-2, E-cadherin, Snail, and Fibronectin in cells examined by Western blot analysis. **G** The YAP1 protein expression and phosphorylation levels of LIMD1 and YAP1 in cells were determined by immunofluorescence staining. **H** The distribution of LIMD1, p-LIMD1, YAP1, and p-YAP1 proteins in the nucleus and cytoplasm was measured by Western blot analysis. **I** The cell viability following transfection detected by CCK-8 assay. **J** The colony formation of cells following transfection. **K, L** The cell cycle entry and cell apoptosis following transfection examined by flow cytometry. $*p < 0.05$, compared with cells transfected with oe-NC; $^{\#}p < 0.05$, compared with cells transfected with oe-YAP1. The results above were measurement data, which were expressed as mean ± standard deviation from three independent experiments. Data between two groups were analyzed by unpaired t-test and data among multiple groups were analyzed by one-way ANOVA with Tukey's post hoc test. Pearson's correlation coefficient was employed to analyze the correlation between phosphorylation levels of LIMD1 and phosphorylation levels of YAP1. Data among multiple groups at different time points were compared by repeated measures ANOVA with Bonferroni's post hoc test.

The results of immunofluorescence staining and confocal microscopy displayed that p-LIMD1 protein and p-YAP1 protein were expressed mainly in the nucleus but also in cytoplasm, while p-CDK1 protein was exclusively expressed in the nucleus. Overexpression of LIMD1 reduced the protein expression of YAP1 and phosphorylation levels of YAP1, suggesting that YAP1 nuclear translocation was inhibited, but overexpressed YAP1 had no influence on phosphorylation levels of LIMD1. In comparison with transfection with oe-YAP1, YAP1 expression was reduced and its

nuclear translocation was inhibited after co-transfection with oe-LIMD1 and oe-YAP1 (Fig. 5G, Supplementary Fig. 2B). The obtained data exhibited the presence of LIMD1 both in the nucleus and cytoplasm, the nuclear location of p-LIMD1 protein and p-YAP1 protein, and additional cytoplasmic location of p-YAP1 protein (Fig. 5H). Overexpression of LIMD1 decreased YAP1 protein expression as well as its nuclear translocation, and overexpression of YAP1 exerted no effect on LIMD1 expression. Compared with oe-YAP1 transfection, co-transfection with oe-LIMD1 and oe-YAP1
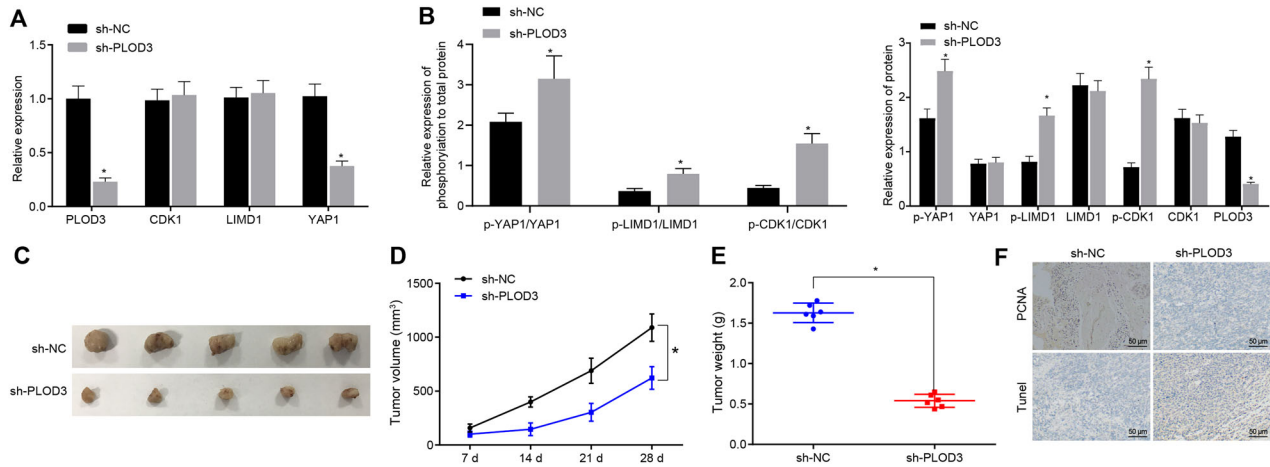
Fig. 6 Silencing of PLOD3 stimulates phosphorylation levels of CDK1 and LIMD1 and reduces YAP1 expression, thus suppressing the tumorigenic ability of NSCLC cells in vivo. A The mRNA expression of PLOD3, CDK1, LIMD1, and YAP1 in transplanted tumor tissues of mice after injection with cells stably transfected with sh-NC or sh-PLOD3, as detected by RT-qPCR. **B** The protein expression of PLOD3, CDK1, LIMD1, YAP1, and their phosphorylation levels in transplanted tumor tissues after silencing PLOD3, as examined by Western blot analysis. **C** Representative images of the transplanted tumors of nude mice injected with the cells transfected with sh-NC or sh-PLOD3. **D** The tumor volume after injection with cells transfected with sh-NC or sh-PLOD3. **E** The tumor weight after injection with cells transfected with sh-NC or sh-PLOD3. **F** The PCNA expression and TUNEL positive cells determined with Immunohistochemistry and TUNEL. $n = 10$ mice in each group. *$p < 0.05$, compared with the tumor in nude mice injected with sh-NC-transfected cells. The results above were measurement data, which were expressed as mean ± standard deviation. Data between two groups were analyzed by t-test and data at different time points were analyzed by one-way ANOVA with Bonferroni's post hoc test.

decreased YAP1 protein expression and its nuclear translocation (Fig. 5H). All these findings led to the conclusion that LIMD1 phosphorylation negatively regulated the expression of YAP1 and its nuclear translocation.

Based on results of CCK-8 assay, colony formation assay, and flow cytometry, overexpressed LIMD1 suppressed the viability and colony formation of A549 cells, but overexpressed YAP1 led to opposite results (both $p < 0.05$). The enhanced cell viability and colony formation of A549 cells by overexpressed YAP1 were normalized by LIMD1 overexpression (Fig. 5I, J Supplementary Fig. 3C), while LIMD1 overexpression induced prolonged G0/G1 phases but shortened S and G2/M phases of A549 cells, and also promoted apoptosis of A549 cells, whereas overexpressed YAP1 contributed to the induction of cell cycle progression and repressed cell apoptosis (all $p < 0.05$). LIMD1 overexpression normalized the promoting effect of YAP1 overexpression on cell cycle progression and its inhibitory effect on cell apoptosis (Fig. 5K, L). We can thus draw the conclusion that LIMD1 phosphorylation downregulated YAP1 expression and its nuclear translocation, thereby blocking the cell cycle entry, repressing cell proliferation, and promoting cell apoptosis of NSCLC.

Silencing of PLOD3 promotes phosphorylation levels of CDK1 and LIMD1, and downregulates YAP1 to inhibit the NSCLC tumorigenesis in vivo

An in vivo xenograft tumor model was developed to analyze the effect of PLOD3 on tumor growth. The stably transfected cells were injected into nude mice, and then RT-qPCR and Western blot analysis was performed to determine the expression of PLOD3, YAP1, CDK1, and LIMD1 in the transplanted tumor tissues. Silencing of PLOD3 led to reduced mRNA and protein expression of PLOD3 and YAP1, but no significant changes were noted in that of CDK1 and LIMD1 (Fig. 6A).

Besides, silencing of PLOD3 obviously enhanced the phosphorylation levels of CDK1 and LIMD1, but inhibited YAP1 protein expression and phosphorylation levels of YAP1 (all $p < 0.05$) (Fig. 6B). Furthermore, PLOD3 knockdown reduced the weight and volume growth of transplanted tumors (Fig. 6C–E), which revealed that loss of PLOD3 suppressed the tumor growth. As

reflected by immunohistochemistry and TUNEL staining (Fig. 6F), a reduction in PCNA expression and increase in positive cells were observed in response to silencing of PLOD3. All in all, silencing of PLOD3 promoted phosphorylation levels of CDK1 and LIMD1, and then downregulated YAP1 expression and suppressed tumor growth of NSCLC in vivo.

DISCUSSION
In spite of the considerable progress made in anti-cancer treatments such as targeted therapies, chemotherapy, and radiotherapy, the five-year survival rate of lung cancer remains dismal[41]. Also, the prognosis of advanced NSCLC remains especially unfavorable[42]. It is established that PLOD3 is an effective initiator of the metastasis of lung cancer and thus presents a promising target for treating NSCLC[5]. We thus explored the role of PLOD3 and the involvement of the PKCδ/CDK1/LIMD1/YAP1 axis in regulating the progression of NSCLC. In a series of experiments, silencing of PLOD3 was observed to activate the PKCδ signaling pathway and then induce the generation of cleaved PKCδ. This in turn promoted phosphorylation levels of CDK1 and LIMD1 but reduced the YAP1 expression, thus suppressing the cell cycle entry and cell proliferation, while enhancing cell apoptosis of NSCLC.

We first found high expression of PLOD3 in NSCLC surgical tissues and cells, and then showed that silencing of PLOD3 generated cleaved PKCδ and then affected the biological function of NSCLC cells. The abnormally high expression of PLOD3 has been documented previously in various cancers. For instance, PLOD3 is upregulated in hepatocellular carcinoma, in which its inactivation exerts tumor-inhibitory effects in vivo and in vitro[23]. Increased expression of PLOD3 in human gastric cancer is strongly associated with larger tumor size and poor prognosis, and suppression of PLOD3 inhibits gastric cancer cell proliferation[43]. PLOD3 silencing suppresses cell proliferation and induces cells cycle arrest at the G1 phase, as well as reducing the migration and invasion of glioma cells by repressing mesenchymal markers, including Snail and Twist[6]. Consistent with those findings, we proved that silencing of PLOD3 suppressed the cell cycle entry, cell proliferation, and tumor

growth and promoted cell apoptosis in NSCLC. Inhibition of PLOD3 has also been reported to suppress human lung cancer cell growth through regulation of the PKCδ signaling pathway, and other research shows that PLOD3 modulates PKC-dependent apoptosis by directly activating PKCα and PKCδ[7]. A previous report also demonstrated that the pro-apoptotic and pro-tumorigenic functions of PKCδ may segregate based on K-Ras dependency, as K-Ras-independent cells are more sensitive to topoisomerase inhibitors, and depletion of PKCδ in this subgroup suppresses apoptosis through increased activation of ERK. In contrast, K-Ras-dependent lung cancer cells are largely insensitive to topoisomerase inhibitors, and depletion of PKCδ can increase apoptosis and decrease activation of ERK in this subgroup[44]. In addition, it was reported that the combined inhibition of PKCδ and EGFR induces marked regression of resistant NSCLC tumors with EGFR mutations[45]. In the line with our findings, a previous study also found a correlation between high expression of PKCδis and the poor prognosis of patients[7]. Partially consistent with those findings, the present study suggested that silencing of PLOD3 activated the PKCδ signaling pathway, promoted the phosphorylation of CDL1/LIMD1, and inhibited YAP1 expression, thus suppressing the progression of NSCLC.

This study demonstrated an upregulation of CDK1 in NSCLC tissues and cells, which has also been found previously in the tumor tissues of lung cancer[46]. Silencing of CDK1 exerts suppressive effects on cell growth, proliferation, migration, and cell cycle entry, but promoted cell apoptosis in NSCLC[47]. Our study also confirmed that upregulated CDK1 phosphorylation exerted a tumor-suppressive function by promoting LIMD1 phosphorylation. In addition, we saw high expression of YAP1 but poor expression of LIMD1 in NSCLC tissues and cells. YAP is an oncogene in various cancers, including lung cancer[48]. As previously reported, YAP1 is an oncogene that is highly-expressed in NSCLC, which could stimulate the proliferation of cancerous cells, thus promoting the occurrence and development of NSCLC[16,38–40,49,50]. Other research has shown that YAP1 acts as a tumor promoter by enhancing tumorigenesis, metastatic potential, and malignant stemness[51]. Silencing YAP1 has been demonstrated to counteract the TGF-β1-provoked epithelial-mesenchymal transition, and the proliferation, migration and invasion processes in NSCLC[50]. Also, YAP1 interacts with SOX5 to stimulate the malignant potential of NSCLC cells, and knockdown of YAP1 impedes the malignant process of NSCLC[39]. Furthermore, LIMD1 has been revealed to usually have poor expression in human lung cancer[13]. Additionally, mitotic phosphorylation of LIMD1 imparts its suppressive role in cell proliferation, cell migration, and invasion[12]. Present findings suggest that LIMD1 phosphorylation downregulates YAP1 expression and its nuclear translocation, thereby preventing progression of NSCLC.

In a previous study, Ophiopogon Saponin C1 has been demonstrated to suppress TNF-α to stabilize endothelium permeability and inhibit lung tumors through PKCδ inhibition[52]. Another report has reported a critical role of nuclear PKCδ as a common axis across multiple known tyrosine kinase inhibitors (TKIs)-resistance mechanisms in EGFR-mutant lung cancer, revealing targeting PKCδ as a therapeutic strategy against heterogeneous mechanisms of EGFR inhibitor resistance in EGFR-mutant lung cancer[45]. In the present study, PLOD3 was observed to be highly expressed in NSCLC tissues and cells. Its knockdown can activate PKCδ protein expression to activate the PKCδ signal pathway, which promotes PKCδ cleavage in a caspase-dependent manner to generate the catalytically active fragment cleaved PKCδ. In turn, cleaved PKCδ can promote CDK1 phosphorylation to upregulate LIMD1 phosphorylation level and inhibit YAP1 expression, thus ultimately blocking cell cycle and preventing the occurrence and development of NSCLC (Fig. 7). This study provides novel insight for further explorations of therapeutic targets involving the PKCδ/CDK1/LIMD1/YAP1 axis for treating NSCLC. Moreover, as introduced by a recent publication[53], small molecule targeting of PLOD3 should be investigated in future
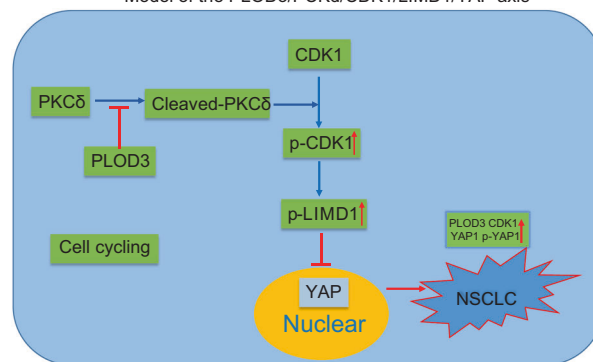

Model of the PLOD3/PCKd/CDK1/LIMD1/YAP axis

Fig. 7 Schematic illustration of the proposed mechanism for NSCLC. Silencing of PLOD3 activates the PKCδ signaling pathway, induces PKCδ cleavage in a caspase-dependent manner, and generates a catalytically active fragment, cleaved PKCδ. Cleaved PKCδ increases phosphorylation levels of CDK1 and LIMD1, while reducing YAP1 expression, ultimately arresting cell cycle and alleviating NSCLC.

in vitro and in vivo studies. In addition, the relevance of targeting the PLOD3 signaling pathway in the NSCLC cell lines warrants further investigation. Besides, in previous researches, it has been reported that AMOTL1 could promote YAP1 translocation and activate the expression of downstream gene CTGF. AMOTL1 plays a carcinogenic role in the occurrence of malignant tumors by interacting with YAP1 and promoting its nuclear accumulation[54]. The interaction between IRF2BP2 and VGLL4 increased the binding of TEAD4 and YAP1, which led to CTGF transcription co-activation, thereby promoting the proliferation, migration, invasion, and epithelial-mesenchymal transition of gastric cancer cells[55]. However, we didn't further study the downstream gene CTGF of YAP1 due to the limited time and funding. In our future study, we will further explore the downstream mechanism.

DATA AVAILABILITY
The authors confirm that the data supporting the findings of this study are available within the article.

REFERENCES
1. Siegel, R. L., Miller, K. D. & Jemal, A. Cancer statistics, 2019. *CA Cancer J Clin* **69**, 7–34 (2019).
2. Ramalingam, S. S., Owonikoko, T. K. & Khuri, F. R. Lung cancer: new biological insights and recent therapeutic advances. *CA Cancer J Clin* **61**, 91–112 (2011).
3. Reck, M. & Rabe, K. F. Precision diagnosis and treatment for advanced non-small-cell lung cancer. *N Engl J Med* **377**, 849–861 (2017).
4. Herbst, R. S., Morgensztern, D. & Boshoff, C. The biology and management of non-small cell lung cancer. *Nature* **553**, 446–454 (2018).
5. Baek, J. H. et al. PLOD3 promotes lung metastasis via regulation of STAT3. *Cell Death Dis* **9**, 1138 (2018).
6. Tsai, C. K. et al. Overexpression of PLOD3 promotes tumor progression and poor prognosis in gliomas. *Oncotarget* **9**, 15705–15720 (2018).
7. Baek, J. H. et al. PLOD3 suppression exerts an anti-tumor effect on human lung cancer cells by modulating the PKC-delta signaling pathway. *Cell Death Dis* **10**, 156 (2019).
8. Reyland, M. E. & Jones, D. N. Multifunctional roles of PKCdelta: opportunities for targeted therapy in human disease. *Pharmacol Ther* **165**, 1–13 (2016).
9. Symonds, J. M., Ohm, A. M., Tan, A. C. & Reyland, M. E. PKCdelta regulates integrin alphaVbeta3 expression and transformed growth of K-ras dependent lung cancer cells. *Oncotarget* **7**, 17905–17919 (2016).
10. LaGory, E. L., Sitailo, L. A. & Denning, M. F. The protein kinase Cdelta catalytic fragment is critical for maintenance of the G2/M DNA damage checkpoint. *J Biol Chem* **285**, 1879–1887 (2010).
11. Li, L., Zhang, Z., Yang, Q. & Ning, M. Lycorine inhibited the cell growth of non-small cell lung cancer by modulating the miR-186/CDK1 axis. *Life Sci* **231**, 116528 (2019).

12. Zhou, J. et al. LIMD1 phosphorylation in mitosis is required for mitotic progression and its tumor-suppressing activity. *FEBS J* **286**, 963–974 (2019).

13. Sharp, T. V. et al. The chromosome 3p21.3-encoded gene, LIMD1, is a critical tumor suppressor involved in human lung cancer development. *Proc Natl Acad Sci USA* **105**, 19932–19937 (2008).

14. Zhang, D. et al. LIMD1 is a survival prognostic marker of gastric cancer and hinders tumor progression by suppressing activation of YAP1. *Cancer Manag Res* **10**, 4349–4361 (2018).

15. Zhu, L. et al. Prognostic significance of nuclear Yes-associated protein 1 in patients with nonsmall cell lung cancer: a systematic review and meta-analysis. *Medicine (Baltimore)* **98**, e15069 (2019).

16. Bora-Singhal, N. et al. YAP1 regulates OCT4 activity and SOX2 expression to facilitate self-renewal and vascular mimicry of stem-like cells. *Stem Cells* **33**, 1705–1718 (2015).

17. Chen, X., Stauffer, S., Chen, Y. & Dong, J. Ajuba phosphorylation by CDK1 promotes cell proliferation and tumorigenesis. *J Biol Chem* **291**, 14761–14772 (2016).

18. Sun, Y. et al. Roles of osteopontin and matrix metalloproteinase-7 in occurrence, progression, and prognosis of nonsmall cell lung cancer. *J Res Med Sci* **20**, 1138–1146 (2015).

19. Feng, J. et al. A novel long noncoding RNA IRAIN regulates cell proliferation in non small cell lung cancer. *Int J Clin Exp Pathol* **8**, 12268–12275 (2015).

20. Trere, D. et al. Prognostic relevance of a novel semiquantitative classification of Bcl2 immunohistochemical expression in human infiltrating ductal carcinomas of the breast. *Ann Oncol* **18**, 1004–1014 (2007).

21. Ellis, I. O. et al. Best Practice No 176: updated recommendations for HER2 testing in the UK. *J Clin Pathol* **57**, 233–237 (2004).

22. Ayuk, S. M., Abrahamse, H. & Houreld, N. N. The role of photobiomodulation on gene expression of cell adhesion molecules in diabetic wounded fibroblasts in vitro. *J Photochem Photobiol B* **161**, 368–374 (2016).

23. Shen, Q. et al. Barrier to autointegration factor 1, procollagen-lysine, 2-oxoglutarate 5-dioxygenase 3, and splicing factor 3b subunit 4 as early-stage cancer decision markers and drivers of hepatocellular carcinoma. *Hepatology* **67**, 1360–1377 (2018).

24. Amodio, G. et al. Identification of a microRNA (miR-663a) induced by ER stress and its target gene PLOD3 by a combined microRNome and proteome approach. *Cell Biol Toxicol* **32**, 285–303 (2016).

25. Chen, X., Lv, Q., Ma, J. & Liu, Y. PLCgamma2 promotes apoptosis while inhibits proliferation in rat hepatocytes through PKCD/JNK MAPK and PKCD/p38 MAPK signalling. *Cell Prolif* **51**, e12437 (2018).

26. Lei, Z. et al. PKCdelta reveals a tumor promoter function by promoting cell proliferation and migration in somatotropinomas. *Int J Clin Exp Pathol* **11**, 208–215 (2018).

27. Xu, L., Su, L. & Liu, X. PKCdelta regulates death receptor 5 expression induced by PS-341 through ATF4-ATF3/CHOP axis in human lung cancer cells. *Mol Cancer Ther* **11**, 2174–2182 (2012).

28. Shi, Y. X. et al. Prognostic and predictive values of CDK1 and MAD2L1 in lung adenocarcinoma. *Oncotarget* **7**, 85235–85243 (2016).

29. Shi, Q. et al. MiR-181a inhibits non-small cell lung cancer cell proliferation by targeting CDK1. *Cancer Biomark* **20**, 539–546 (2017).

30. Chen, X. et al. The Cdc2/Cdk1 inhibitor, purvalanol A, enhances the cytotoxic effects of taxol through Op18/stathmin in non-small cell lung cancer cells in vitro. *Int J Mol Med* **40**, 235–242 (2017).

31. Qiu, X. G. et al. Functional BCL-2 rs2279115 promoter noncoding variant contributes to glioma predisposition, especially in males. *DNA Cell Biol* **38**, 85–90 (2019).

32. Kaspar, M., Zardi, L. & Neri, D. Fibronectin as target for tumor therapy. *Int J Cancer* **118**, 1331–1339 (2006).

33. Beltran, M. et al. A natural antisense transcript regulates Zeb2/Sip1 gene expression during Snail1-induced epithelial-mesenchymal transition. *Genes Dev* **22**, 756–769 (2008).

34. Schimizzi, G. V. & Longmore, G. D. Ajuba proteins. *Curr Biol* **25**, R445–R446 (2015).

35. Das Thakur, M. et al. proteins are negative regulators of the Hippo signaling pathway. *Curr Biol* **20**, 657–662 (2010).

36. Ibar, C., Kirichenko, E., Keepers, B., Enners, E., Fleisch, K. & Irvine, K. D. Tension-dependent regulation of mammalian Hippo signaling through LIMD1. *J Cell Sci* **131**, jcs214700 (2018).

37. Xiao, X. et al. LncRNA ENST00000453774.1 contributes to oxidative stress defense dependent on autophagy mediation to reduce extracellular matrix and alleviate renal fibrosis. *J Cell Physiol* **234**, 9130–9143 (2019).

38. Jin, D. et al. The antineoplastic drug metformin downregulates YAP by interfering with IRF-1 binding to the YAP promoter in NSCLC. *EBioMedicine* **37**, 188–204 (2018).

39. Zou, H. et al. SOX5 interacts with YAP1 to drive malignant potential of non-small cell lung cancer cells. *Am J Cancer Res* **8**, 866–878 (2018).

40. Huang, C. et al. MiR-497 suppresses YAP1 and inhibits tumor growth in non-small cell lung cancer. *Cell Physiol Biochem* **37**, 342–352 (2015).

41. Leon, G., MacDonagh, L., Finn, S. P., Cuffe, S. & Barr, M. P. Cancer stem cells in drug resistant lung cancer: targeting cell surface markers and signaling pathways. *Pharmacol Ther* **158**, 71–90 (2016).

42. Majem, B., Nadal, E. & Munoz-Pinedo, C. Exploiting metabolic vulnerabilities of Non small cell lung carcinoma. *Semin Cell Dev Biol* **98**, 54–62 (2020).

43. Wang, B. et al. PLOD3 is upregulated in gastric cancer and correlated with clinicopathologic characteristics. *Clin Lab* **65**, https://doi.org/10.7754/Clin.Lab.2018.180541 (2019).

44. Ohm, A. M., Tan, A. C., Heasley, L. E. & Reyland, M. E. Co-dependency of PKCdelta and K-Ras: inverse association with cytotoxic drug sensitivity in KRAS mutant lung cancer. *Oncogene* **36**, 4370–4378 (2017).

45. Lee, P. C. et al. Targeting PKCdelta as a therapeutic strategy against heterogeneous mechanisms of EGFR inhibitor resistance in EGFR-mutant lung cancer. *Cancer Cell* **34**, 954–969 e4 (2018).

46. Zhang, C. et al. Loss of cytoplasmic CDK1 predicts poor survival in human lung cancer and confers chemotherapeutic resistance. *PLoS One* **6**, e23849 (2011).

47. Jacquot, C. et al. Cucurbitacin-D-induced CDK1 mRNA up-regulation causes proliferation arrest of a non-small cell lung carcinoma cell line (NSCLC-N6). *Anticancer Res* **34**, 4797–4806 (2014).

48. Lo Sardo, F., Strano, S. & Blandino, G. YAP and TAZ in lung cancer: oncogenic role and clinical targeting. Cancers (Basel). **10**, 137 (2018).

49. Chen, M. J., Wang, Y. C., Wu, D. W., Chen, C. Y. & Lee, H. Association of nuclear localization of SHP2 and YAP1 with unfavorable prognosis in non-small cell lung cancer. *Pathol Res Pract* **215**, 801–806 (2019).

50. Yu, M. et al. YAP1 contributes to NSCLC invasion and migration by promoting Slug transcription via the transcription co-factor TEAD. *Cell Death Dis* **9**, 464 (2018).

51. Shibata, M. & Hoque, M. O. Targeting cancer stem cells: a strategy for effective eradication of cancer. Cancers (Basel). **11**, 732 (2019).

52. Zhang, Y. et al. Ophiopogon Saponin C1 inhibits lung tumors by stabilizing endothelium permeability via Inhibition of PKCdelta. *Int J Biol Sci* **16**, 396–407 (2020).

53. Kim, I. W. et al. Computational drug repositioning for gastric cancer using reversal gene expression profiles. *Sci Rep* **9**, 2660 (2019).

54. Zhou, Y. et al. AMOTL1 enhances YAP1 stability and promotes YAP1-driven gastric oncogenesis. *Oncogene* **39**, 4375–4389 (2020).

55. Yao, Y. et al. Down-regulation of interferon regulatory factor 2 binding protein 2 suppresses gastric cancer progression by negatively regulating connective tissue growth factor. *J Cell Mol Med* **23**, 8076–8089 (2019).

AUTHOR CONTRIBUTIONS

W.H.L., F.B.W. and K.H. participated in the conception and design of the study. F.B.W., G.H.C. and H.Z.G. performed the analysis and interpretation of data. H.Z.G., G.H.C. and S.Z. contributed to drafting the article. W.H.L. and S.Z. revised it critically for important intellectual content. All authors have read and approved the final submitted manuscript.

COMPETING INTERESTS

The authors declare no competing interests.

ETHICS APPROVAL AND CONSENT TO PARTICIPATE

The study was approved by the Ethics Committee of the First Affiliated Hospital of Zhengzhou University. Written informed consent was obtained from all participants in accordance with the Declaration of Helsinki. All animal experiments were carried out in accordance with the Guide for the Care and Use of Laboratory Animals published by the US National Institutes of Health.

ADDITIONAL INFORMATION

Supplementary information The online version contains supplementary material available at https://doi.org/10.1038/s41374-021-00674-7.

Correspondence and requests for materials should be addressed to Song Zhao.

Reprints and permission information is available at http://www.nature.com/reprints

Publisher's note Springer Nature remains neutral with regard to jurisdictional claims in published maps and institutional affiliations.